

Two-Phase Spray Cooling of Hybrid Vehicle Electronics

Preprint

I. Mudawar
Mudawar Thermal Systems

D. Bharathan, K. Kelly, and S. Narumanchi
National Renewable Energy Laboratory

*Presented at Itherm 2008
Orlando, Florida
May 28–31, 2008*

Conference Paper
NREL/CP-540-42389
July 2008

NREL is operated by Midwest Research Institute • Battelle Contract No. DE-AC36-99-GO10337



NOTICE

The submitted manuscript has been offered by an employee of the Midwest Research Institute (MRI), a contractor of the US Government under Contract No. DE-AC36-99GO10337. Accordingly, the US Government and MRI retain a nonexclusive royalty-free license to publish or reproduce the published form of this contribution, or allow others to do so, for US Government purposes.

This report was prepared as an account of work sponsored by an agency of the United States government. Neither the United States government nor any agency thereof, nor any of their employees, makes any warranty, express or implied, or assumes any legal liability or responsibility for the accuracy, completeness, or usefulness of any information, apparatus, product, or process disclosed, or represents that its use would not infringe privately owned rights. Reference herein to any specific commercial product, process, or service by trade name, trademark, manufacturer, or otherwise does not necessarily constitute or imply its endorsement, recommendation, or favoring by the United States government or any agency thereof. The views and opinions of authors expressed herein do not necessarily state or reflect those of the United States government or any agency thereof.

Available electronically at <http://www.osti.gov/bridge>

Available for a processing fee to U.S. Department of Energy and its contractors, in paper, from:

U.S. Department of Energy
Office of Scientific and Technical Information
P.O. Box 62
Oak Ridge, TN 37831-0062
phone: 865.576.8401
fax: 865.576.5728
email: <mailto:reports@adonis.osti.gov>

Available for sale to the public, in paper, from:

U.S. Department of Commerce
National Technical Information Service
5285 Port Royal Road
Springfield, VA 22161
phone: 800.553.6847
fax: 703.605.6900
email: orders@ntis.fedworld.gov
online ordering: <http://www.ntis.gov/ordering.htm>



TWO-PHASE SPRAY COOLING OF HYBRID VEHICLE ELECTRONICS

Issam Mudawar
Mudawar Thermal Systems Inc., 1291 Cumberland Avenue
West Lafayette, IN 47906, USA
Phone and Fax: (765) 463-6516
Email: im@mudawar.com

and

Desikan Bharathan, Kenneth Kelly, Sreekant Narumanchi
National Renewable Energy Laboratory, 1617 Cole Boulevard
Golden, CO 80401, USA

ABSTRACT

As part of the U.S. Department of Energy (DOE) Advanced Power Electronics (APE) program, DOE's National Renewable Energy Laboratory (NREL) is currently leading a national effort to develop next-generation cooling technologies for hybrid vehicle electronics. Spray cooling has been identified as a potential solution that can dissipate 150–200 W/cm² while maintaining the chip temperature below 125°C. This study explores the viability and implementation of this cooling scheme. First, commercial coolants are assessed for their suitability to this application in terms of thermal, environmental, and safety concerns and material compatibility. In this assessment, HFE-7100 is identified as the optimum coolant in all performance categories. Next, spray models are used to determine the HFE-7100 spray conditions that meet such stringent heat dissipation requirements. These findings are verified experimentally, demonstrating that spray cooling is a viable thermal management solution for hybrid vehicle electronics.

KEY WORDS: hybrid vehicles, power electronics, electronics cooling, spray cooling, environmental

NOMENCLATURE

A, A' area
 B nucleate boiling coefficient
 Bo boiling number
 c_p specific heat
 d_{32} Sauter mean diameter (SMD)
 d_o nozzle orifice diameter
 H orifice-to-surface distance
 h_{fg} latent heat of vaporization
 k thermal conductivity
 L length and width of square test surface
 P pressure
 ΔP pressure drop across spray nozzle
 Pr Prandtl number
 P_{sat} saturation pressure
 Q volumetric flow rate
 $\overline{Q''}$ local volumetric spray flux
 $\overline{Q''}$ average volumetric spray flux based on circular impact area of spray
 q_m'' average critical heat flux based on total area of square surface
 $q_{m,p}''$ local critical heat flux

q_s'' device heat flux
 r radial distance from centerline of spray
 Re_{d_o} Reynolds number based on nozzle orifice diameter
 T temperature
 T_f nozzle inlet temperature
 T_s surface temperature
 T_{sat} saturation temperature
 ΔT_{sub} difference between saturation temperature and nozzle inlet temperature,
 $T_{sat} - T_f$
 We_{d_o} Weber number based on nozzle orifice diameter

Greek Symbols

γ angular coordinate in volumetric flux model
 θ spray cone angle
 μ viscosity
 ρ density
 σ surface tension

Subscripts

d_o based on diameter of nozzle orifice
 f liquid; nozzle inlet
 g vapor
 m maximum (critical heat flux, CHF)
 p point-based
 s surface
 sat saturation
 sub subcooling.

INTRODUCTION

Near-Term and Long-Term Transitions in Vehicle Technology

Achieving energy independence ultimately depends on successfully developing hybrid electric and fuel cell vehicles that are economically justifiable to the average consumer. This will require reducing the production cost of current automotive electric traction systems by a factor of four. Thus, the size of the systems will have to be reduced by more than 50%, and greater modularity will be needed to support increases in system configurations and economies of scale [1]. For the technology to be successfully adopted, system integration will also be essential to reduce the part count and to improve reliability, durability, and producibility.

In recent years, we have witnessed unprecedented interest in the development of a new electric propulsion system to facilitate the transitioning from conventional engines to economical combustion engine hybrid vehicles in the near term and to fuel cell vehicles in the long term. To achieve these goals, a major collaborative effort was launched through the FreedomCAR and Fuel Partnership, which include the U.S. Department of Energy (DOE), BP America, Chevron Corporation, ConocoPhillips, Exxon Mobil Corporation, Shell Hydrogen LLC, and the United States Council for Automotive Research, a legal partnership among DaimlerChrysler Corporation, Ford Motor Company, and General Motors Corporation [1].

Interestingly, electrical propulsion systems are already available in the market, but their use is hindered by their cost—about \$33/kW, which amounts to \$1,815 for a complete 55-kW system [1]. The goal, then, in developing new electric propulsion systems is to decrease their cost to a level that renders hybrid and fuel cell vehicles economically justifiable for consumers. As shown in Fig. 1, DOE’s target is to reduce the cost of an electric propulsion system (which includes an electric traction motor, inverter, and voltage booster) to \$12/kW by 2015 and \$8/kW by 2020. This would bring the total cost of the system to \$660 by 2015 and \$440 by 2020.

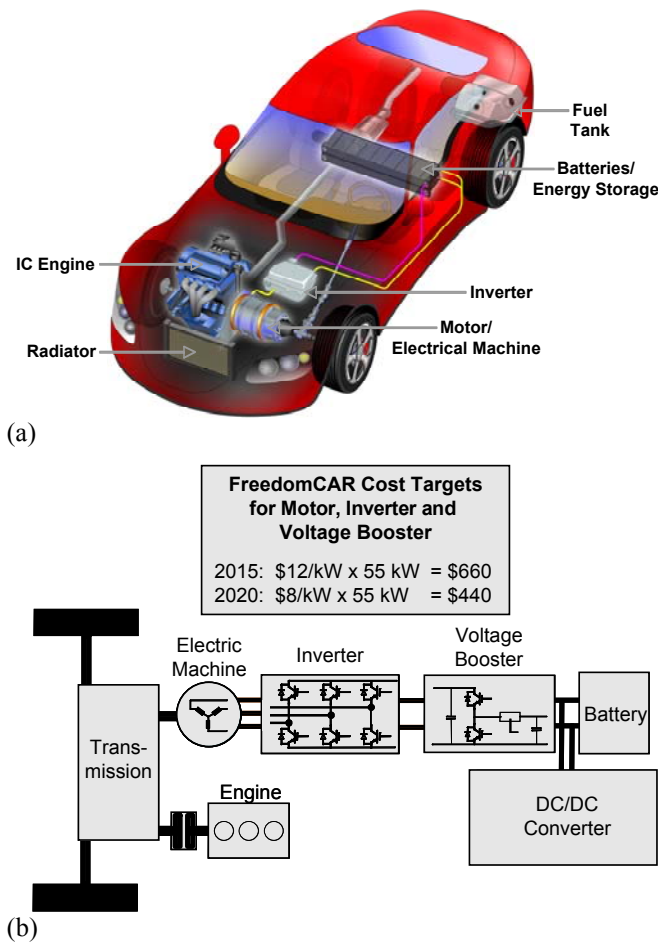


Fig. 1 (a) Propulsion system components for hybrid vehicle; (b) parallel hybrid vehicle configuration (adapted from [2]) and FreedomCAR cost targets [1].

The Role of Thermal Management

To successfully integrate power electronics and electric machines into an electronics system, various thermal characteristics and performance targets must be met along with reducing the weight, volume, and cost of the electronic components. Thermal management plays a vital role in the pursuit of these goals.

The National Renewable Energy Laboratory (NREL) currently leads research and development activities in thermal control as part of DOE’s Advanced Power Electronics and Electrical Machines program. The overall objective of the thermal control activities is to develop advanced technologies and effective integrated thermal control systems that meet DOE’s FreedomCAR program goals. The following are some key barriers in the development of thermal control technologies.

- Existing thermal control techniques are not adequate for dissipating high heat fluxes while limiting the operation of silicon-based electronic components to a temperature of less than 125°C.
- Current components are generally both bulky and heavy, resulting in the need for additional structural support and increased use of parasitic power.
- Material and processing technologies remain too costly for use in the automotive industry.

To achieve FreedomCAR goals, significant advances must be achieved in the thermal control of both the power electronics and motors. By optimizing existing technologies and extending them to new pioneering cooling methods, NREL aims to achieve higher power densities, smaller volumes and weights, and increased reliability for the drivetrain components. These efforts will also lead to lower costs for the new technologies, so they can be implemented in the automotive industry.

The current study was performed by a partnership consisting of Mudawar Thermal Systems Inc. under a subcontract from NREL to develop advanced thermal management solutions that utilize spray cooling to dissipate 150-200 W/cm² from silicon-based electronic devices in hybrid vehicles while maintaining device temperature below 125°C. While the use of trench insulated-gate bipolar transistors (IGBTs), which are silicon-based and can withstand up to 150°C, is becoming more prevalent in inverters, the use of a lower maximum temperature of 125°C was deemed more appropriate for thermal management system design.

SELECTING A THERMAL MANAGEMENT SOLUTION Direct versus Indirect Liquid Cooling

Achieving the aforementioned heat flux dissipation and device temperature is highly dependent on chip packaging. Virtually all existing hybrid vehicle cooling work centers on indirect liquid cooling of the chip as illustrated in Fig. 2(a). Cooling performance in this case is only partially dictated by the convective boundary. Because of the resistances of the different layers of materials separating the chip from the liquid coolant, a relatively large temperature gradient is incurred when dissipating high heat fluxes. These resistances may be completely eliminated by direct liquid cooling of the chip. However, having liquid come in direct contact with the chip’s surface limits cooling options to a few dielectric and inert coolants. Unfortunately, the thermophysical properties of

these coolants are quite inferior to those of common coolants such as water/ethylene glycol. Direct liquid cooling is therefore advantageous only when its convective thermal resistance is smaller than the sum of the convective, conductive and contact resistances of the indirect cooling configuration illustrated in Fig. 2(a). Because heat spreading plays a minor role in a direct cooling system, high-flux chips may be packaged quite close to one another, greatly reducing both the weight and the volume of the cooling system.

Given the inferior thermophysical properties of dielectric coolants and the strong dependence of cooling performance on convective resistance, the viability of a direct cooling system is highly dependent on the ability to achieve very large convective heat transfer coefficients. As shown in Fig. 2(b), this goal can be realized by adopting a highly effective liquid cooling configuration (*e.g.*, spray, jet impingement, micro-channel flow) and also by capitalizing on the benefits of phase change.

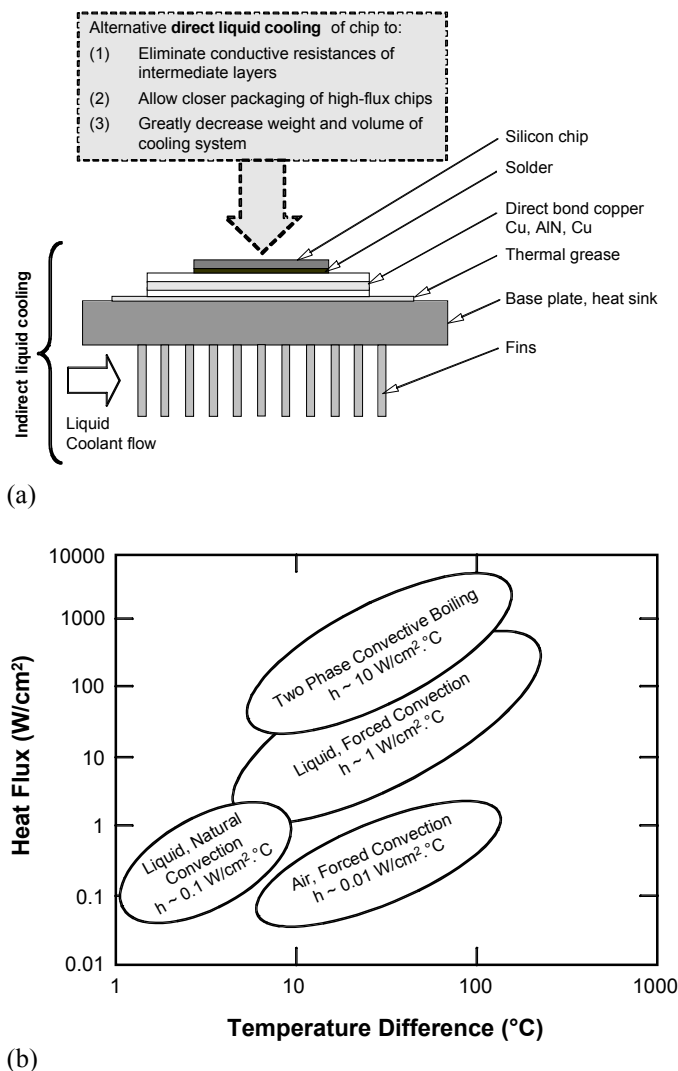


Fig. 2 (a) Cooling path for removing heat from silicon die using indirect cooling with water/ethylene glycol, and alternative direct liquid cooling; (b) capabilities of existing cooling technologies using various fluids and operating pressures.

The primary objective of this study is to explore the effectiveness of direct two-phase spray cooling in meeting the heat flux and temperature requirements of future hybrid vehicle electronics.

Spray Cooling

High-flux electronic cooling applications demand the use of specialized types of sprays-pressure sprays-that utilize liquid momentum rather than a secondary air stream to break up the liquid into fine droplets. A large increase in the liquid's surface-area-to-volume ratio is achieved that, coupled with the broad dispersion of droplets across the heat-dissipating surface, both increases the spray's convective high heat transfer coefficient and helps to ensure the surface temperature uniformity demanded by electronic devices [3].

Toda [4] observed that subcooling the spray liquid had minor effects on single-phase and nucleate boiling heat transfer and did not have a dominant effect on critical heat flux (CHF). Both Toda [4] and Monde [5] showed that spray volumetric flux, Q'' , has by far the strongest effect on cooling performance. Volumetric flux is defined as the flow rate of spray liquid impacting an infinitesimal portion of the surface divided by the area of the same portion; it has the units of velocity.

Cho and Wu [6] developed a CHF correlation for Freon-113 sprays based on Weber number but did not account for droplet size. Mudawar and Valentine [7] determined local cooling characteristics for all regimes of the boiling curve for water. Like Toda and Monde, they showed that volumetric flux had the most dominant effect on spray cooling. Estes and Mudawar [8] developed an empirical relation for CHF for FC-72, FC-87 and water based on local volumetric flux, Q'' , and Sauter mean diameter (SMD), d_{32} , but not droplet speed. However, Chen *et al.* [9] concluded that d_{32} has a negligible effect on CHF, while droplet velocity is a dominant parameter in the determination of CHF.

There are many barriers to implementing sprays to cool high-flux electronic devices. These barriers stem mostly from poor understanding of spray cooling compared with competing options such as jet-impingement. There are also practical concerns resulting from the lack of repeatability of cooling performance for seemingly identical nozzles because of minute manufacturing imperfections or due to corrosion or erosion of the nozzle's interior passages [10].

Cooling Loop Options

Two different cooling loop configurations are considered for possible implementation of spray cooling. As shown in Fig. 3(a), the first consists of modifying the vehicle's refrigeration loop with a pump-assisted sub-loop containing a spray-cooling chamber in which the heat is removed from the vehicle electronics. Figure 3(b) shows an alternative configuration, in which the electronics are cooled by a separate loop using an appropriate coolant.

The modified refrigeration loop configuration requires using the same coolant currently employed in the primary loop, R134a. Pressure in this loop is set at about 2069 kPa (300 psia) and the coolant temperature at the saturation temperature for R134a corresponding to the same pressure. With a separate loop, there is far greater flexibility in selecting the coolant, operating pressure and, hence, coolant temperature. However, a maximum pressure of about 2069

kPa (300 psia) is desired for the separate loop as well to preclude excessive system weight. The pressure must also be maintained above ambient to prevent air inclusion in the event of a system leak. Such an inclusion can lead to a substantial deterioration in the condenser's performance as well as induce cavitation inside the pump.

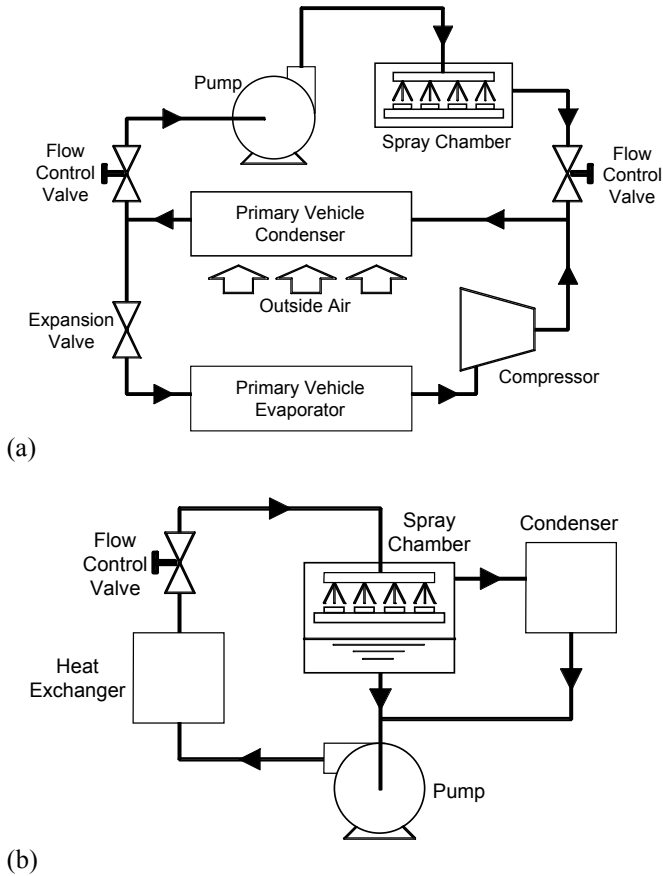


Fig. 3 Cooling of hybrid vehicle power electronics by (a) modifying existing R134a air-conditioning refrigeration loop and (b) using a separate cooling loop with appropriate coolant.

Other important parameters concern the spray chamber itself. The primary heat dissipation requirement is to remove $150\text{--}200\text{ W/cm}^2$ while maintaining the chip temperature below 125°C .

With a typical device-to-coolant temperature drop of about 30°C in the nucleate boiling regime for spray cooling [8], the coolant temperature should be maintained below 95°C . Since the saturation temperature is the highest possible coolant temperature for a coolant intended for phase-change cooling, we can conclude that the saturation temperature of the coolant corresponding to the spray chamber pressure should be below 95°C as well.

Another temperature limit concerns the condenser. As a result of phase change, the coolant temperature inside the condenser remains close to the saturation temperature as the vapor is gradually converted to liquid. The condenser is cooled externally by ambient air. Recent calculations at NREL reveal that the log-mean temperature difference between the coolant and air is about 30°C . For a relatively

high ambient air temperature of 30°C , this implies that the coolant saturation temperature in the condenser must be no less than 60°C . Therefore, the saturation temperature in the separate loop must satisfy the criterion $60 < T_{sat} < 95^\circ\text{C}$ and the pressure be maintained in the range of $101.3\text{--}2069\text{ kPa}$ ($14.7\text{--}300\text{ psia}$).

Coolant Selection

Thermal requirements represent only one aspect of the task of selecting an appropriate coolant. Other crucial requirements include high dielectric strength, inertness and material compatibility, safety, and environmental concerns. Two different types of coolant are considered, refrigerants and liquid coolants; the latter are fluids that maintain a liquid state at atmospheric pressure. Both types of coolants are examined based on the following criteria:

- *Dielectric strength*: The highest voltage that can be sustained across a layer of the fluid before fluid breakdown or arcing takes place,
- *Dielectric constant*: The amount of electrostatic energy that can be stored per unit volume of fluid when a unit voltage is applied,
- *Flammability*: The susceptibility of the fluid to ignite, either spontaneously or as a result of a spark or open flame,
- *Auto-ignition temperature*: The temperature at which fluid would self-ignite,
- *Lower explosive limit (LEL)*: The concentration of fluid for a given volume of air that renders a mixture flammable or explosive,
- *Atmospheric lifetime*: The time required for fluid concentration in the atmosphere to drop to $1/e$ of its initial value,
- *Ozone depletion potential (ODP)*: A relative index indicating the extent to which the fluid may cause ozone depletion; the highest value, 1.0, is assigned to the highly ozone-depleting R11,
- *Global warming potential (GWP)*: Indicates how much a given mass of the refrigerant contributes to global warming over a 100-year period compared with the same mass of CO_2 ; the latter is assigned a GWP value of 1.0.

A recent comprehensive study [11] grouped these performance criteria into general categories, including environmental, safety, dielectric strength, and material compatibility. The environmental rating is based on ODP and GWP. A *good* rating corresponds to zero ODP and a GWP of less than 1500, an *average* rating indicates $0.1 > \text{ODP} > 0$ or $6000 > \text{GWP} > 1500$, and a *poor* rating indicates $\text{ODP} > 0.1$ or $\text{GWP} > 6000$. The safety rating is based on flammability. A coolant is rated *good* if it is nonflammable and *poor* if it is flammable.

There are three main families of refrigerants. The earliest to be introduced were chlorofluorocarbons (CFCs) (e.g., R11, R12, R113 and R114), which are composed of chlorine, fluorine and carbon. While CFCs are both nontoxic and inert, they are highly ozone-depleting and contribute to global warming. Hydrochlorofluorocarbons (HCFCs) (e.g., R123, R124 and R141b) constitute a more recent alternative to CFCs, given their somewhat similar inertness and cooling characteristics but less than 10% of the ozone-depleting effects of CFCs. More recently, a new family of refrigerants, hydrofluorocarbons (HFCs) (e.g., R134a and R143a) have

been introduced that provide essentially zero ozone depletion and reduced global warming effects.

As discussed earlier, the desired operating saturation pressure-temperature ($P_{sat}-T_{sat}$) plane is 101.3–2069 kPa (14.7–300 psia) and 60–95°C, respectively. Figure 4(a) shows that 13 of the refrigerants fall in the desired $P_{sat}-T_{sat}$ plane. Four of these (R141b, R152a, R600 and R600a) have *poor* safety ratings because of their flammability. All remaining nine refrigerants have *good* ratings in this category. Four CFCs (R11, R113, R114 and R12) and one HFC (R236fa) have *poor* ratings in the environmental category and have already been phased out by the Montreal Protocol because of their high ODP [12]. In contrast, R236fa has zero ODP but very high GWP. All three HCFCs (R123, R124 and R141b) in Fig. 4(a) have *average* environmental ratings because of their non-zero ODP. Refrigerants with *good* environmental ratings include two HFCs (R134a and R245fa) and two hydrocarbons (R600 and R600a). Overall, only R134a and R245fa have received good ratings in most categories. Of these two, only R134a has complete published thermophysical properties.

A similar fluid assessment was conducted for liquid coolants [11]. These include the following families of fluids: 3M Fluorinert (FCs), 3M Novec (HFCs), 3M Performance (FCs), Certonal, Solvay HT and ZT, Cooper Environtemp and Tranelec, Paratherm NF, Dow Corning OS-120, and Intech EDM. A key obstacle in using many of these coolants is the shortage of thermophysical property data; only 3M fluids come with detailed property information. The 3M coolants include perfluorocarbons (PFCs) (Fluorinerts FC-72, FC-87 and FC-84, and Performance Fluids PF-5050, PF-5052, PF-5060 and PF-5070), and HFCs (Novec fluids HFE-7100 and HFE-7200).

Figure 4(b) shows that 12 of the 3M liquid coolants fall in the desired $P_{sat}-T_{sat}$ plane. All 3M liquid coolants have *good* safety ratings, though HFE-7200 carries a low LEL. However, Fluorinerts (FC-72, FC84, FC-87) and Performance Fluids (PF-5050, PF-5052, PF-5060 and PF-5070) have only *average* environmental ratings because of their relatively high GWP. Overall, only HFE-7100 has *good* ratings in all performance categories. It is important to note that the freeze point for HFE-7100 is -135°C, which is well below any expected automobile application range of temperatures down to -40°C.

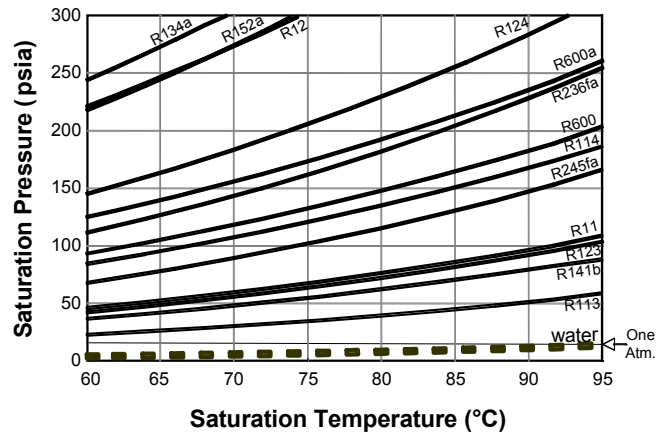
Based on this coolant assessment study, one refrigerant, R134a, and one liquid coolant, HFE-7100, are deemed suitable for cooling hybrid vehicle electronics. In the following section, we consider the spray cooling performance of these two coolants.

SPRAY COOLING PERFORMANCE PREDICTIONS

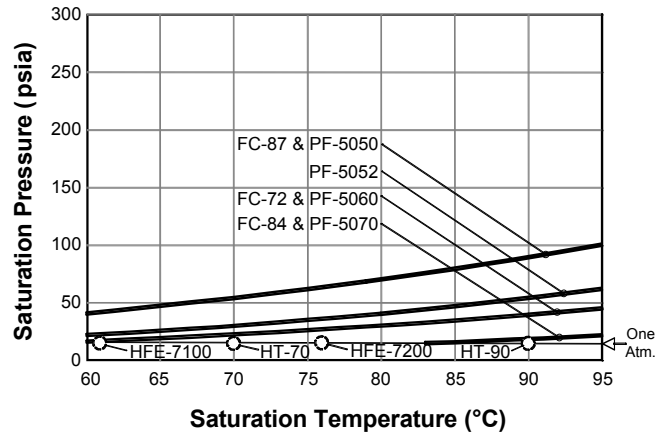
Spray Configuration and Predictive Relations

Two spray parameters have significant influence on nucleate boiling heat transfer performance and CHF: volumetric flux, Q'' , and Sauter mean diameter, d_{32} . While d_{32} is fairly uniform across the spray, Q'' for full-cone spray nozzles (which are favored for electronic cooling applications) exhibits significant spatial variations.

Mudawar and Estes [13] provided a detailed study of the spatial variation of volumetric flux for a full-cone spray nozzle. They modeled the nozzle orifice as a uniform point source for fluid flow. Figure 5 shows that a constant



(a)



(b)

Fig. 4 Pressure-temperature saturation characteristics for (a) refrigerants and (b) liquid coolants (characteristics for some of the liquids are available over the entire temperature range; for others, saturation temperatures are available only at one atmosphere).

volumetric flux along a spherical surface of radius equal to the orifice-to-surface distance would yield a nonuniform volumetric flux distribution along the heated surface. The model yielded the following expression for local volumetric flux, Q'' , along the heated surface:

$$\frac{Q''}{\bar{Q}''} = \frac{1}{2} \left[\frac{\tan^2(\theta/2)}{1 - \cos(\theta/2)} \right] \left[\frac{1}{1 + \left(\frac{r}{H} \right)^2} \right]^{3/2}, \quad (1)$$

where \bar{Q}'' is the mean volumetric flux across the impact area,

$$\bar{Q}'' = \frac{Q}{\pi \{H \tan(\theta/2)\}^2}. \quad (2)$$

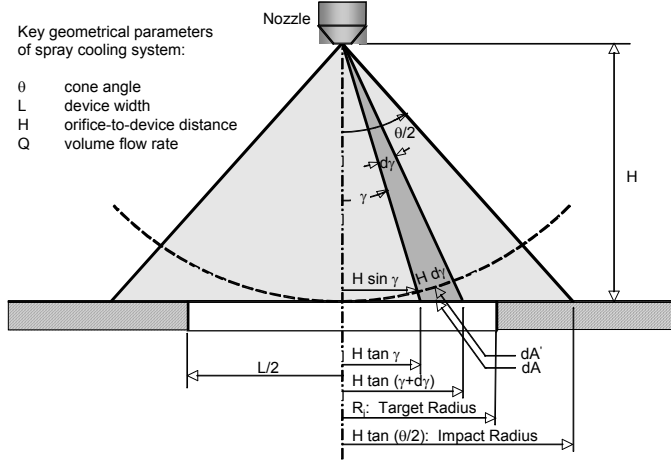
This model predicts a higher flow rate at the center of the spray impact area in comparison to the circumference of the same area. The spatial variations of Q'' have a strong bearing on both cooling uniformity and CHF. The relatively low volumetric flux in the outer regions means that CHF would commence at the circumference. Mudawar and Estes [13] demonstrated experimentally how a large orifice-to-surface distance causes a significant portion of the spray droplets to fall outside of the heated area. Conversely, a small distance

results in a small droplet impact area, depriving much of the heated test surface of the advantages of direct droplet impact. Both extremes yield relatively low CHF values, and *CHF is highest when the impact area just inscribes the square heated surface, i.e., when*

$$H \tan(\theta/2) = L/2 \quad (3)$$

and

$$\bar{Q}'' = Q / (\pi L^2 / 4). \quad (4)$$



Optimum configuration (impact radius equal to device width): $L/2 = H \tan(\theta/2)$

Fig. 5 Point-source model of volumetric flux distribution for pressure spray nozzle.

Estes and Mudawar [8] used the orifice diameter, d_o , and liquid velocity at the orifice, $(2\Delta P/\rho_f)^{0.5}$, to represent the characteristic length and velocity, respectively, for full cone spray nozzles. They correlated Sauter mean diameter data for FC-72, FC-87 and water according to the relation

$$\frac{d_{32}}{d_o} = 3.67 [We_{d_o}^{1/2} Re_{d_o}]^{0.259}, \quad (5)$$

where We_{d_o} and Re_{d_o} are defined, respectively, as

$$We_{d_o} = \frac{\rho_g (2\Delta P / \rho_f) d_o}{\sigma} \quad (6)$$

and

$$Re_{d_o} = \frac{\rho_f (2\Delta P / \rho_f)^{1/2} d_o}{\mu_f}. \quad (7)$$

Recently, Rybicki and Mudawar [14] combined their upward-oriented PF-5052 spray data with the downward-oriented water spray data of Mudawar and Valentine [7] to derive the following nucleate boiling correlation

$$Bo^* = 4.79 \times 10^{-3} \left(\frac{c_{p,f} (T_s - T_f)}{h_{fg}} \right)^{5.75}, \quad (8)$$

where

$$Bo^* = \frac{\left(\frac{q_s'' d_{32}}{\mu_f h_{fg}} \right)}{\left(\frac{\rho_f}{\rho_g} \right)^{2.5} \left(\frac{\rho_f \bar{Q}'' d_{32}}{\sigma} \right)^{0.35}}. \quad (9)$$

Using their data for FC-72 and FC-87 along with Mudawar and Valentine's [7] water data, Estes and Mudawar [8] developed the following correlation for *local* CHF along the outer edge of the impact area, $q_{m,p}''$, based on volumetric spray flux along the same edge:

$$\frac{q_{m,p}''}{\rho_g h_{fg} \bar{Q}''} = 2.3 \left(\frac{\rho_f}{\rho_g} \right)^{0.3} \left(\frac{\rho_f \bar{Q}'' d_{32}}{\sigma} \right)^{-0.35} \left(1 + 0.0019 \frac{\rho_f c_{p,f} \Delta T_{sub}}{\rho_g h_{fg}} \right). \quad (10)$$

Equation (10) can be used to determine the measured CHF data (based on the total area of a square test surface) in terms of the mean volumetric flux according to the following transformation:

$$q_{m,p}'' = q_m'' \frac{L^2}{\left(\frac{\pi L^2}{4} \right)} = \frac{4}{\pi} q_m'' \quad (11)$$

and

$$\frac{Q''}{\bar{Q}''} = \frac{1}{2} \{1 + \cos(\theta/2)\} \cos(\theta/2). \quad (12)$$

Equation (12) is derived by substituting $r = H \tan(\theta/2)$ in Eq. (1).

Predictions

As indicated earlier, only conditions falling in the pressure range of one atmosphere to $P_{sat} = 2069$ kPa (300 psi) and saturation temperature range of $T_{sat} = 60$ -95°C are considered for the hybrid vehicle application. To achieve temperatures in excess of 60°C with R134a, high pressures between 1700 and 2067 kPa are required. As shown in Table 1, the corresponding saturation temperature range is fairly narrow, between 60 and 68.9°C. Thus, two representative temperatures are examined for R134a, one corresponding to each limit of this temperature range. Table 1 provides all relevant thermophysical properties corresponding to these temperatures.

As shown in Table 1, HFE-7100 provides a fairly broad range of saturation temperatures, from $T_{sat} = 60.4$ °C at one atmosphere to $T_{sat} = 95.0$ °C corresponding to a pressure of 275.9 kPa. In other words, this coolant spans virtually the entire operating temperature range for hybrid vehicles at moderate to mild operating pressures. Five representative temperatures are examined for this coolant, spanning the range of 60.4 to 95°C. Table 1 provides all relevant thermophysical properties corresponding to these temperatures.

The spray cooling relations discussed in the previous section are used to predict the cooling performances of three full-cone spray nozzles used in previous studies by Mudawar and Estes [13] and Rybicki and Mudawar [14]. Table 2 provides values for orifice diameter, d_o , and spray angle, θ , for each of these nozzles.

The thermal performance results for R134a and HFE-7100 are presented in the form of (1) the relationship between heat flux, q_s'' , and surface temperature, T_s , in the nucleate boiling regime, and (2) CHF value. Notice that the relationship between q_s'' and T_s , which is given by Eqs. (8) and (9), can be expressed for a given nozzle at each saturation temperature and flow rate as

$$q_s'' = B (T_s - T_f)^{5.75}. \quad (13)$$

Table 3 shows the thermal performance results for R134a. Because of the small temperature range possible with this

Table 1. Operating conditions and corresponding thermophysical properties used in thermal analysis.

Spray chamber constraints:
 $60 < T_{\text{sat}} < 95 \text{ }^\circ\text{C}$ & $101.3 < P_{\text{sat}} < 2069 \text{ kPa}$

| R134a | | | | |
|----------------------------------|--|----------------------------|------------------------|----------------------------------|
| Sat. Pressure | Sat. Temp. | Latent Heat of Vap. | Liquid Specific Heat | Liquid Density |
| P_{sat} (kPa) | T_{sat} ($^\circ\text{C}$) | h_{fg} (kJ/kg) | $C_{p,f}$ (kJ/kg.K) | ρ_f (kg/m ³) |
| 1700 | 60.0 | 138.8 | 1.669 | 1052 |
| 2069 ^a | 68.9 | 126.0 | 1.791 | 1002 |
| Vapor Density | Liquid Viscosity | Liquid Thermal Conduct. | Liquid Prandtl Number | Surface Tension |
| ρ_g (kg/m ³) | μ_f (kg/m.s) | k_f (W/m.K) | Pr_f | σ (N/m) |
| 88.69 | 0.000124 | 0.0647 | 3.18 | 0.0037 |
| 112.67 | 0.000109 | 0.0594 | 3.27 | 0.0027 |

a 2069 kPa = 300 psia, maximum allowable spray chamber pressure

| HFE-7100 | | | | |
|----------------------------------|--|----------------------------|------------------------|----------------------------------|
| Sat. Pressure | Sat. Temp. | Latent Heat of Vap. | Liquid Specific Heat | Liquid Density |
| P_{sat} (kPa) | T_{sat} ($^\circ\text{C}$) | h_{fg} (kJ/kg) | $C_{p,f}$ (kJ/kg.K) | ρ_f (kg/m ³) |
| 101.3 ^b | 60.4 | 112.1 | 1.254 | 1372 |
| 119.0 | 65.0 | 110.5 | 1.263 | 1359 |
| 159.6 | 75.0 | 107.0 | 1.283 | 1329 |
| 211.4 | 85.0 | 103.4 | 1.303 | 1299 |
| 275.9 | 95.0 | 99.7 | 1.323 | 1269 |
| Vapor Density | Liquid Viscosity | Liquid Thermal Conduct. | Liquid Prandtl Number | Surface Tension |
| ρ_g (kg/m ³) | μ_f (kg/m.s) | k_f (W/m.K) | Pr_f | σ (N/m) |
| 9.66 | 0.000355 | 0.0619 | 7.19 | 0.0117 |
| 11.26 | 0.000339 | 0.0610 | 7.02 | 0.0114 |
| 14.94 | 0.000306 | 0.0590 | 6.65 | 0.0105 |
| 19.61 | 0.000279 | 0.0571 | 6.36 | 0.0096 |
| 25.47 | 0.000256 | 0.0551 | 6.13 | 0.0088 |

b 101.3 kPa = 1 atm

Table 2. Spray nozzle parameters.

| Nozzle | d_0 (m) | θ ($^\circ$) |
|--------|-----------------------|-----------------------|
| 1 | 0.76×10^{-3} | 55.8 |
| 2 | 1.19×10^{-3} | 46.4 |
| 3 | 1.70×10^{-3} | 48.5 |

coolant, subcooling values range from 0 to only 8.9°C. This small range is a cause for concern since spray formation requires a minimum of 10°C to produce repeatable, fully developed droplet breakup [13]. The flow rate ranges indicated in Table 3 are those that were shown by Mudawar and Estes to produce fully developed droplet breakup. Overall, values of the nucleate boiling coefficient B are quite small, which corresponds to large surface-to-fluid temperature differences. A measurable increase in the magnitude of B is realized at the higher of the two saturation pressures. CHF values for this coolant are surprisingly large, exceeding the required heat flux of 200 W/cm². Table 3 shows that CHF increases with increasing flow rate, but it is slightly smaller at the higher of the two pressures. Comparing values for $\Delta T_{\text{sub}} = 8.9^\circ\text{C}$ and $\Delta T_{\text{sub}} = 0^\circ\text{C}$ at 2069 kPa shows that, while CHF does increase with subcooling, this effect is quite weak for sprays. Overall, the large CHF values for R134a may be attributed to the high pressure attainable with this coolant at relatively low coolant temperatures. However, substituting the calculated B values and $q_s = 200 \text{ W/cm}^2$ in Eq. (13) yields surface temperatures that exceed the maximum allowable temperature of 125°C. This indicates that spray cooling with R134a may not meet the stated goals of 200 W/cm² while maintaining surface temperatures below 125°C.

Table 4 shows the thermal results for HFE-7100, which spans virtually the entire saturation temperature range allowed in a hybrid vehicle cooling loop. This facilitates using this coolant over a broad range of pressures, temperatures and subcoolings, evidenced by the relatively large number of cases examined in Table 4. Overall, values of B are far greater than those for R134a, meaning *HFE-7100 can maintain far smaller device surface temperatures than R134a can*. Substituting these B values in Eq. (13) shows that this coolant can maintain device temperatures below the maximum allowable temperature of 125°C even when dissipating 200 W/cm². The magnitude of B increases with increasing flow rate and decreasing pressure. Table 4 shows that CHF for HFE-7100 exceeds 200 W/cm² at saturation temperatures of 85°C or greater (the shaded values in Table 4). Table 4 indicates that *CHF increases appreciably with increasing flow rate, but only mildly with increasing subcooling and/or pressure*.

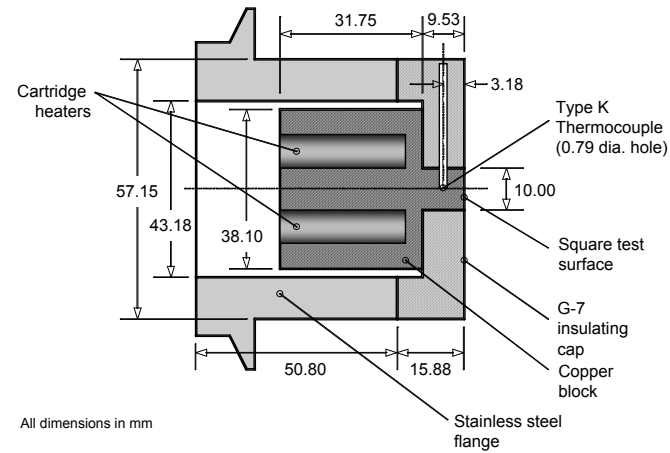
Given the inability of R134a to maintain the required device temperatures and the positive results of HFE-7100, validation experiments were performed with the latter fluid. In the next section, we describe the experimental methods used and discuss the results of the validation study.

EXPERIMENTAL VALIDATION

Test Facility

Figure 6 illustrates the construction of a test heater that was used to simulate chip heat dissipation to a spray. The test heater consists of a 1.0 x 1.0 cm² square surface protruding from a large cylindrical oxygen-free copper block. The test surface is surrounded with insulating G-7 fiberglass plastic. The back of the copper block is bored to accept three high-power electrical cartridge heaters. To minimize heat loss, the outer surface of the copper block is covered with high temperature ceramic insulation. The entire heater assembly is attached to a stainless steel flange for mounting to a test vessel. A thermocouple is inserted a short distance behind the square test surface, from which the surface temperature is determined. The test heater's heat flux is determined by

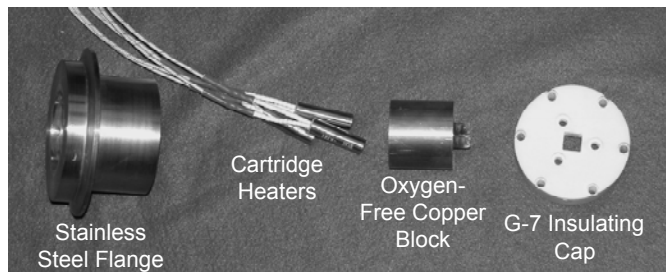
dividing electrical power input by the square area of the test surface. Maximum heat loss is estimated at less than 7% of the electrical power input.



(a)



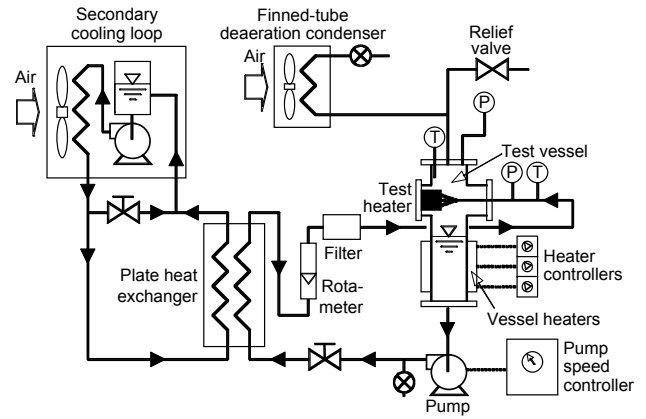
(b)



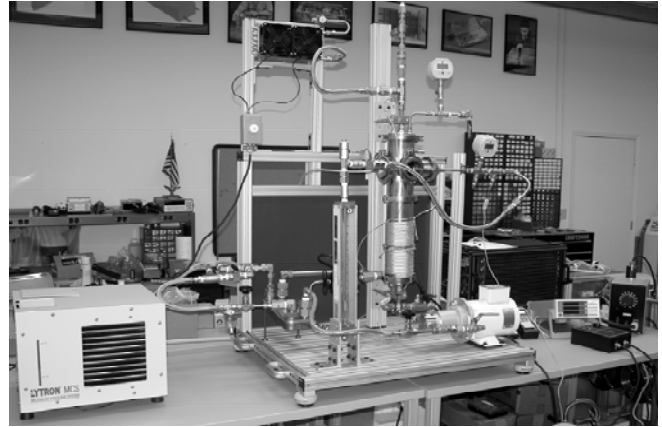
(c)

Fig. 6 (a) Construction of test heater; (b) photo of heater assembly depicting square test surface centered in G-7 insulating cap; (c) photos of individual test heater parts.

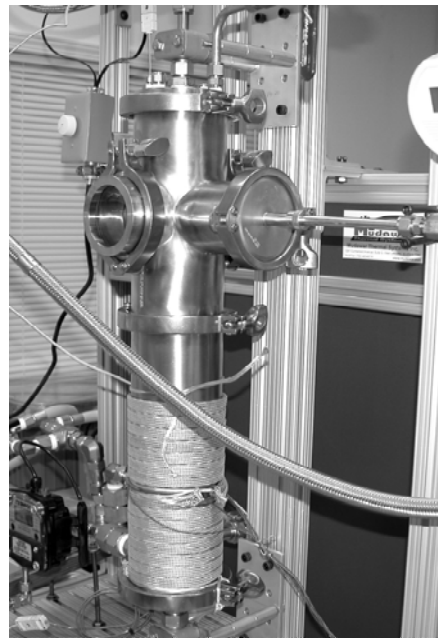
Figure 7 depicts the two-phase flow loop that is designed to deliver the test fluid at the desired pressure, temperature and flow rate to the spray nozzle located inside the loop's test chamber. The coolant is partially evaporated upon impact with the test heater. The remaining liquid accumulates in the bottom of the test vessel, while the vapor is separated from it by buoyancy into the vessel's top region. As illustrated in Fig. 7(a), liquid from the test vessel drains directly to a gear pump.



(a)



(b)



(c)

Fig. 7 (a) Schematic of flow loop; (b) photo of test facility; (c) photo of test vessel.

The pumped liquid passes through a regulating valve followed by a plate-type heat exchanger, where the fluid is subcooled. The heat is rejected to water circulating through the plate heat exchanger. This water is supplied from a pump contained in a secondary liquid-to-air cooler with a self-contained reservoir. The heat absorbed by the water is rejected to an air-cooled finned-tube heat exchanger integral to the liquid-to-air cooler. Exiting the plate heat exchanger, the primary liquid flows through a rotameter followed by an in-line filter before returning to the spray nozzle. A separate air-cooled finned-tube heat exchanger is situated above the test vessel for deaeration purposes.

The working fluid is deaerated for about 45 minutes before each series of experiments. The fluid is first poured into the test vessel and the pump started to circulate the fluid through the loop. The test heater, which is located inside the test vessel, and three wrap-around test vessel heaters are then turned on. A mixture of the test fluid's vapor and air accumulates in the upper region of the test vessel; from there it is routed by buoyancy into the finned-tube heat exchanger. The vapor is recaptured by condensation as noncondensable gases are purged to the ambient. Following the deaeration process, the flow loop is sealed completely from the ambient to maintain the working fluid's purity during the thermal tests.

All tests are performed with the spray orifice situated from the test surface according to Eq. (3), such that the spray impact area just inscribes the square test surface in order to achieve the highest possible CHF. For a given spray flow rate, the desired saturation pressure inside the test vessel as well as liquid subcooling at the nozzle inlet are achieved by simultaneously regulating heat input to the test vessel's wrap-around heaters and water flow through the plate-type heat exchanger. Boiling data are generated by supplying electrical power to the test heater's cartridge heaters in small increments that are each followed by a 30- to 40-minute waiting period to allow the test surface to reach steady-state temperature. Experiments are terminated when an unsteady rise in the test heater temperature signals the commencement of CHF.

Uncertainties in the pressure, flow rate and temperature measurements are less than 0.25%, 2.0% and $\pm 0.1^\circ\text{C}$, respectively.

Experimental Results

CHF was found in the previous section to increase appreciably with increasing flow rate but only mildly with increasing subcooling and/or pressure. Therefore, all the validation tests were performed with nozzle 3 (see Table 3), which provides, for the same pressure drop, the largest flow rate of the three nozzles examined earlier.

Figure 8 shows boiling curves obtained for nozzle 3 at different flow rates, pressures and subcoolings. The tested range for each of these parameters is broken into *high*, *medium*, and *low* subranges. Note that the boiling curves tend to cluster in the nucleate boiling region. Large variations in CHF are primarily the result of flow rate variations and, to a far lesser extent, subcooling or pressure variations. In fact, all four *high* flow rate cases successfully meet the hybrid vehicle cooling requirements. Notice how CHF values for these cases exceed 200 W/cm^2 at surface temperatures safely below 125°C . On the other hand, *medium* and *low* flow rates fail to reach the 200 W/cm^2 level, although surface temperatures at CHF for these cases are below 125°C .

| Test # | Flow Rate | Pressure | Subcooling | CHF |
|--------|---|--|----------------------------------|---|
| 1 | High ($1.305 \times 10^{-5}\text{ m}^3/\text{s}$) (0.207 gpm) | Low ($1.44 \times 10^5\text{ N/m}^2$) (20.9 psia) | High (38.5°C) | 263 W/cm^2 |
| 2 | High ($1.305 \times 10^{-5}\text{ m}^3/\text{s}$) (0.207 gpm) | Medium ($1.71 \times 10^5\text{ N/m}^2$) (24.8 psia) | Low (24.6°C) | 205 W/cm^2 at 105.8°C |
| 3 | High ($1.160 \times 10^{-5}\text{ m}^3/\text{s}$) (0.184 gpm) | Low ($1.36 \times 10^5\text{ N/m}^2$) (19.7 psia) | High (36.8°C) | 245 W/cm^2 at 110.4°C |
| 4 | Medium ($0.725 \times 10^{-5}\text{ m}^3/\text{s}$) (0.115 gpm) | Low ($1.36 \times 10^5\text{ N/m}^2$) (19.7 psia) | High (39.2°C) | 194 W/cm^2 at 104.1°C |
| 5 | High ($1.160 \times 10^{-5}\text{ m}^3/\text{s}$) (0.184 gpm) | Medium ($1.64 \times 10^5\text{ N/m}^2$) (23.8 psia) | High (41.9°C) | --- |
| 6 | High ($1.051 \times 10^{-5}\text{ m}^3/\text{s}$) (0.167 gpm) | Medium ($1.77 \times 10^5\text{ N/m}^2$) (25.6 psia) | High (43.0°C) | 255 W/cm^2 at 109.6°C |
| 7 | Low ($0.353 \times 10^{-5}\text{ m}^3/\text{s}$) (0.056 gpm) | High ($2.14 \times 10^5\text{ N/m}^2$) (31.3 psia) | High (56.1°C) | 175 W/cm^2 at 116.0°C |
| 8 | Low ($0.372 \times 10^{-5}\text{ m}^3/\text{s}$) (0.059 gpm) | Low ($1.42 \times 10^5\text{ N/m}^2$) (17.8 psia) | High (40.6°C) | 138 W/cm^2 at 97.9°C |

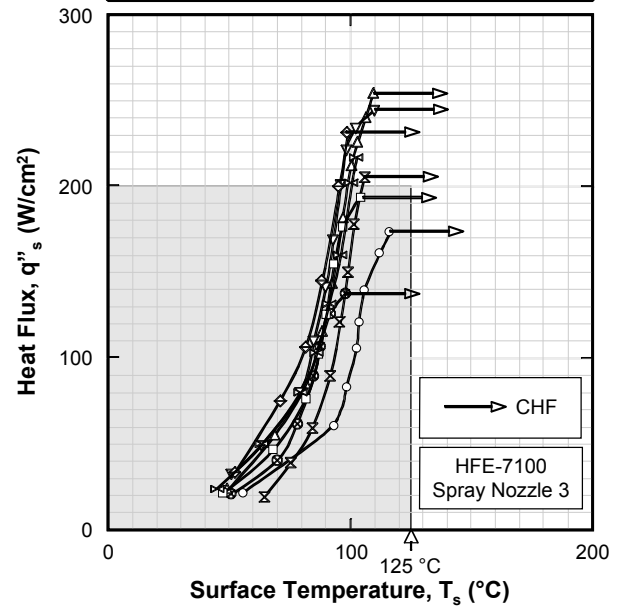


Fig. 8 Boiling curves from thermal tests.

Figure 9 compares measured and predicted CHF for all the validation tests. Overall, the data are slightly higher than predicted, but trends relative to flow rate, subcooling and pressure appear to be correctly captured.

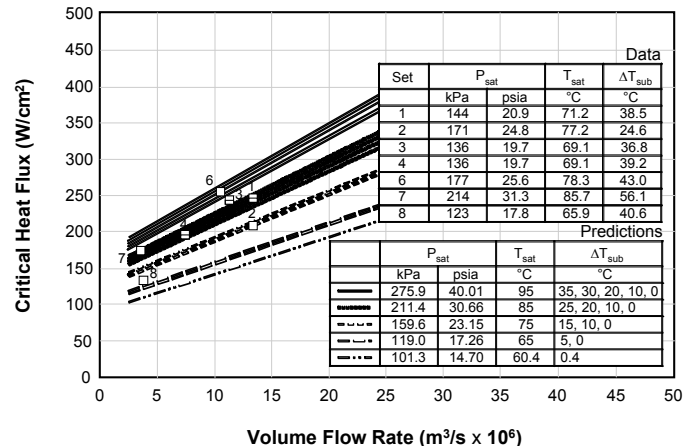


Fig. 9 Comparison of CHF predictions and experimental data.

These findings demonstrate that spray cooling is a viable approach that can meet the stringent thermal management requirements of hybrid vehicles.

SUMMARY AND CONCLUSIONS

This study explored thermal management solutions for high-flux electronics in hybrid vehicles. Different cooling systems were considered along with a comprehensive assessment of the suitability of different refrigerants and liquid coolants to this application. Recent models were reviewed and integrated into a systematic methodology for predicting the cooling performance of pressure spray nozzles. This methodology was used to explore the effectiveness of two-phase sprays and identify an optimum coolant. It also identifies desired ranges of spray parameters that could safely dissipate 150–200 W/cm² while maintaining the chip temperature below 125°C. Finally, those predictions were validated experimentally. The key conclusions of this study are as follows:

- (1) Different refrigerants and liquid coolants were assessed relative to the desired pressure–temperature operation envelope for hybrid vehicle electronics. This also included evaluating the coolants' environmental impact, dielectric properties, safety, and material compatibility, as well as determining the availability of detailed thermophysical property data. Only hydrofluorocarbons (HFCs) scored well in all these performance categories. Of the HFCs, one refrigerant, R134a, and one liquid coolant, HFE-7100, show the greatest promise.
- (2) The predictive methodology for two-phase spray cooling shows that R134a can yield CHF values that greatly exceed the heat fluxes anticipated in hybrid vehicle electronics. However, this coolant is not capable of maintaining device temperatures below the maximum allowable temperature of 125°C when dissipating 200 W/cm². With HFE-7100, several operating conditions were identified that yield CHF values in excess of 200 W/cm² and surface temperatures below 125°C.
- (3) The attractive performance of HFE-7100 was validated experimentally for different flow rates, subcoolings and pressures. These tests prove that CHF is sensitive primarily to flow rate and, to a far lesser extent, subcooling and pressure. High flow rate tests exceed the 200 W/cm² heat flux requirement at surface temperatures safely below 125°C. These findings demonstrate the viability of HFE-7100 spray cooling in terms of meeting the thermal management requirements of hybrid vehicles.

Acknowledgement: This work was supported through National Renewable Energy Laboratory Subcontract YEV-6-55511-01 under the U.S. Department of Energy Contract DE-AC36-99GO10337.

REFERENCES

- [1] Electrical and Electronics Technical Team, *Electrical and Electronics Technical Team Roadmap*, U.S. Department of Energy, Washington, DC, 2006.
- [2] K. Bennion, 2007, *Plug-in Hybrid Electric Vehicle Impacts on Power Electronics and Electric Machines*, National Renewable Energy Laboratory report NREL/MP-540-36085, Golden, CO, 2007.
- [3] I. Mudawar, "Assessment of High-Heat-Flux Thermal Management Schemes," *IEEE Trans.-CPMT: Components Packaging Tech.*, Vol. 24, pp. 122-141, 2001.
- [4] S. Toda, "A Study in Mist Cooling (1st Report: Investigation of Mist Cooling)," *Trans. JSME*, Vol. 38, pp. 581-588, 1972.
- [5] M. Monde, "Critical Heat Flux in Saturated Forced Convection Boiling with an Impinging Droplet," *Trans. JSME*, Vol. 46, pp. 1146-1155, 1980.
- [6] C.S.K. Cho and K. Wu, "Comparison of Burnout Characteristics in Jet Impingement Cooling and Spray Cooling," *Proc. Nat. Heat Transfer Conf.*, Houston, Texas, pp. 561-567, 1988.
- [7] I. Mudawar and W.S. Valentine, "Determination of the Local Quench Curve for Spray-Cooled Metallic Surfaces," *J. Heat Treating*, Vol. 7, pp. 107-121, 1989.
- [8] K.A. Estes and I. Mudawar, "Correlation of Sauter Mean Diameter and Critical Heat Flux for Spray Cooling of Small Surfaces," *Int. J. Heat Mass Transfer*, Vol. 38, pp. 2985-2996, 1995.
- [9] R.-H. Chen, L.C. Chow and J.E. Navedo, "Effects of Spray Characteristics on Critical Heat Flux in Subcooled Water Spray Cooling," *Int. J. Heat Mass Transfer*, Vol. 45, pp. 4033-4043, 2002.
- [10] D.D. Hall and I. Mudawar, "Experimental and Numerical Study of Quenching Complex-Shaped Metallic Alloys with Multiple, Overlapping Sprays," *Int. J. Heat Mass Transfer*, Vol. 38, pp. 1201-1216, 1995.
- [11] I. Mudawar, *Spray Cooling of Power Electronics*, technical report to the National Renewable Energy Laboratory, West Lafayette, IN, 2006.
- [12] I.H. Rowlands, "The Fourth Meeting of the Parties to the Montreal Protocol: Report and Reflection," *Environment*, Vol. 35, pp. 25-34, 1993.
- [13] I. Mudawar and K.A. Estes, "Optimizing and Predicting CHF in Spray Cooling of a Square Surface," *J. Heat Transfer*, Vol. 118, pp. 672-680, 1996.
- [14] J.R. Rybicki and I. Mudawar, "Single-Phase and Two-Phase Cooling Characteristics of Upward-Facing and Downward-Facing Sprays," *Int. J. Heat Mass Transfer*, Vol. 49, pp. 5-12, 2006.

Table 3. Predicted cooling performance for R134a.

| P _{sat} (kPa) | T _{sat} (°C) | T _f (°C) | ΔT _{sub} (°C) | Q (m ³ /s) | | | B | | | CHF (W/m ²) | | | T _s (°C) at 200 W/cm ² | | |
|---------------------------|--------------------------|------------------------|---------------------------|--------------------------|-----------------------|-----------------------|-----------------------|-----------------------|-----------------------|----------------------------|----------------------|----------------------|--|----------|----------|
| | | | | Nozzle 1 | Nozzle 2 | Nozzle 3 | Nozzle 1 | Nozzle 2 | Nozzle 3 | Nozzle 1 | Nozzle 2 | Nozzle 3 | Nozzle 1 | Nozzle 2 | Nozzle 3 |
| 1700 | 60 | 60 | 0 | 4.0x10 ⁻⁶ | 8.0x10 ⁻⁶ | 12.0x10 ⁻⁶ | 2.06x10 ⁻⁶ | 2.53x10 ⁻⁶ | 2.84x10 ⁻⁶ | 6.74x10 ⁶ | 7.32x10 ⁶ | 7.48x10 ⁶ | 181.54 | 177.27 | 174.94 |
| | | | | 6.0x10 ⁻⁶ | 12.0x10 ⁻⁶ | 18.0x10 ⁻⁶ | 3.14x10 ⁻⁶ | 3.86x10 ⁻⁶ | 4.32x10 ⁻⁶ | 8.19x10 ⁶ | 8.89x10 ⁶ | 9.08x10 ⁶ | 172.95 | 168.97 | 166.85 |
| | | | | 8.0x10 ⁻⁶ | 16.0x10 ⁻⁶ | 24.0x10 ⁻⁶ | 4.23x10 ⁻⁶ | 5.20x10 ⁻⁶ | 5.83x10 ⁻⁶ | 9.40x10 ⁶ | 10.2x10 ⁶ | 10.4x10 ⁶ | 167.25 | 163.46 | 161.43 |
| 2069 | 68.9 | 60 | 8.9 | 4.0x10 ⁻⁶ | 8.0x10 ⁻⁶ | 12.0x10 ⁻⁶ | 2.42x10 ⁻⁶ | 3.00x10 ⁻⁶ | 3.36x10 ⁻⁶ | 6.85x10 ⁶ | 7.44x10 ⁶ | 7.63x10 ⁶ | 178.18 | 173.85 | 171.63 |
| | | | | 6.0x10 ⁻⁶ | 12.0x10 ⁻⁶ | 18.0x10 ⁻⁶ | 3.69x10 ⁻⁶ | 4.57x10 ⁻⁶ | 5.12x10 ⁻⁶ | 8.33x10 ⁶ | 9.04x10 ⁶ | 9.27x10 ⁶ | 169.82 | 165.81 | 163.74 |
| | | | | 8.0x10 ⁻⁶ | 16.0x10 ⁻⁶ | 24.0x10 ⁻⁶ | 4.98x10 ⁻⁶ | 6.16x10 ⁻⁶ | 6.90x10 ⁻⁶ | 9.57x10 ⁶ | 10.4x10 ⁶ | 10.6x10 ⁶ | 164.24 | 160.46 | 158.50 |
| | 68.9 | 0 | 4.0x10 ⁻⁶ | 8.0x10 ⁻⁶ | 12.0x10 ⁻⁶ | 2.42x10 ⁻⁶ | 3.00x10 ⁻⁶ | 3.36x10 ⁻⁶ | 6.71x10 ⁶ | 7.28x10 ⁶ | 7.48x10 ⁶ | 187.08 | 182.75 | 180.53 | |
| | | | 6.0x10 ⁻⁶ | 12.0x10 ⁻⁶ | 18.0x10 ⁻⁶ | 3.69x10 ⁻⁶ | 4.57x10 ⁻⁶ | 5.12x10 ⁻⁶ | 8.16x10 ⁶ | 8.85x10 ⁶ | 9.08x10 ⁶ | 178.72 | 174.71 | 172.64 | |
| | | | 8.0x10 ⁻⁶ | 16.0x10 ⁻⁶ | 24.0x10 ⁻⁶ | 4.98x10 ⁻⁶ | 6.16x10 ⁻⁶ | 6.90x10 ⁻⁶ | 9.37x10 ⁶ | 10.2x10 ⁶ | 10.4x10 ⁶ | 173.14 | 169.36 | 167.40 | |

Table 4. Predicted cooling performance for HFE 7100.

| P _{sat} (kPa) | T _{sat} (°C) | T _f (°C) | ΔT _{sub} (°C) | Q (m ³ /s) | | | B | | | CHF (W/m ²) | | | T _s (°C) at 200 W/cm ² | | |
|---------------------------|--------------------------|------------------------|---------------------------|--------------------------|-----------------------|-----------------------|-----------------------|-----------------------|-----------------------|----------------------------|----------------------|----------------------|--|----------|----------|
| | | | | Nozzle 1 | Nozzle 2 | Nozzle 3 | Nozzle 1 | Nozzle 2 | Nozzle 3 | Nozzle 1 | Nozzle 2 | Nozzle 3 | | Nozzle 2 | Nozzle 3 |
| 101.3 | 60.4 | 60 | 0.4 | 4.0x10 ⁻⁶ | 8.0x10 ⁻⁶ | 12.0x10 ⁻⁶ | 7.58x10 ⁻⁴ | 9.32x10 ⁻⁴ | 10.5x10 ⁻⁴ | 1.36x10 ⁶ | 1.48x10 ⁶ | 1.51x10 ⁶ | CHF | CHF | CHF |
| | | | | 6.0x10 ⁻⁶ | 12.0x10 ⁻⁶ | 18.0x10 ⁻⁶ | 11.5x10 ⁻⁴ | 14.2x10 ⁻⁴ | 16.0x10 ⁻⁴ | 1.66x10 ⁶ | 1.80x10 ⁶ | 1.84x10 ⁶ | CHF | CHF | CHF |
| | | | | 8.0x10 ⁻⁶ | 16.0x10 ⁻⁶ | 24.0x10 ⁻⁶ | 15.5x10 ⁻⁴ | 19.1x10 ⁻⁴ | 21.5x10 ⁻⁴ | 1.90x10 ⁶ | 2.06x10 ⁶ | 2.11x10 ⁶ | CHF | 97.04 | 96.29 |
| 119.0 | 65 | 60 | 5 | 4.0x10 ⁻⁶ | 8.0x10 ⁻⁶ | 12.0x10 ⁻⁶ | 5.49x10 ⁻⁴ | 6.76x10 ⁻⁴ | 7.58x10 ⁻⁴ | 1.52x10 ⁶ | 1.65x10 ⁶ | 1.68x10 ⁶ | CHF | CHF | CHF |
| | | | | 6.0x10 ⁻⁶ | 12.0x10 ⁻⁶ | 18.0x10 ⁻⁶ | 8.36x10 ⁻⁴ | 10.3x10 ⁻⁴ | 11.5x10 ⁻⁴ | 1.84x10 ⁶ | 2.01x10 ⁶ | 2.05x10 ⁶ | CHF | 101.24 | 100.46 |
| | | | | 8.0x10 ⁻⁶ | 16.0x10 ⁻⁶ | 24.0x10 ⁻⁶ | 11.3x10 ⁻⁴ | 13.9x10 ⁻⁴ | 15.5x10 ⁻⁴ | 2.12x10 ⁶ | 2.30x10 ⁶ | 2.35x10 ⁶ | 100.58 | 99.15 | 98.41 |
| | 65 | 0 | 4.0x10 ⁻⁶ | 8.0x10 ⁻⁶ | 12.0x10 ⁻⁶ | 5.49x10 ⁻⁴ | 6.76x10 ⁻⁴ | 7.58x10 ⁻⁴ | 1.50x10 ⁶ | 1.63x10 ⁶ | 1.66x10 ⁶ | CHF | CHF | CHF | |
| | | | 6.0x10 ⁻⁶ | 12.0x10 ⁻⁶ | 18.0x10 ⁻⁶ | 8.36x10 ⁻⁴ | 10.3x10 ⁻⁴ | 11.5x10 ⁻⁴ | 1.82x10 ⁶ | 1.98x10 ⁶ | 2.02x10 ⁶ | CHF | CHF | 105.46 | |
| | | | 8.0x10 ⁻⁶ | 16.0x10 ⁻⁶ | 24.0x10 ⁻⁶ | 11.3x10 ⁻⁴ | 13.9x10 ⁻⁴ | 15.5x10 ⁻⁴ | 2.09x10 ⁶ | 2.27x10 ⁶ | 2.32x10 ⁶ | 105.58 | 104.15 | 103.41 | |
| 159.6 | 75 | 60 | 15 | 4.0x10 ⁻⁶ | 8.0x10 ⁻⁶ | 12.0x10 ⁻⁶ | 3.14x10 ⁻⁴ | 3.88x10 ⁻⁴ | 4.35x10 ⁻⁴ | 1.81x10 ⁶ | 1.98x10 ⁶ | 2.02x10 ⁶ | CHF | CHF | 107.91 |
| | | | | 6.0x10 ⁻⁶ | 12.0x10 ⁻⁶ | 18.0x10 ⁻⁶ | 4.79x10 ⁻⁴ | 5.90x10 ⁻⁴ | 6.62x10 ⁻⁴ | 2.20x10 ⁶ | 2.40x10 ⁶ | 2.45x10 ⁶ | 107.12 | 105.44 | 104.54 |
| | | | | 8.0x10 ⁻⁶ | 16.0x10 ⁻⁶ | 24.0x10 ⁻⁶ | 6.45x10 ⁻⁴ | 7.95x10 ⁻⁴ | 8.92x10 ⁻⁴ | 2.54x10 ⁶ | 2.75x10 ⁶ | 2.81x10 ⁶ | 104.74 | 103.14 | 102.29 |
| | 65 | 10 | 4.0x10 ⁻⁶ | 8.0x10 ⁻⁶ | 12.0x10 ⁻⁶ | 3.14x10 ⁻⁴ | 3.88x10 ⁻⁴ | 4.35x10 ⁻⁴ | 1.80x10 ⁶ | 1.96x10 ⁶ | 2.00x10 ⁶ | CHF | CHF | 112.91 | |
| | | | 6.0x10 ⁻⁶ | 12.0x10 ⁻⁶ | 18.0x10 ⁻⁶ | 4.79x10 ⁻⁴ | 5.90x10 ⁻⁴ | 6.62x10 ⁻⁴ | 2.18x10 ⁶ | 2.38x10 ⁶ | 2.43x10 ⁶ | 112.12 | 110.44 | 109.54 | |
| | | | 8.0x10 ⁻⁶ | 16.0x10 ⁻⁶ | 24.0x10 ⁻⁶ | 6.45x10 ⁻⁴ | 7.95x10 ⁻⁴ | 8.92x10 ⁻⁴ | 2.51x10 ⁶ | 2.72x10 ⁶ | 2.78x10 ⁶ | 109.74 | 108.14 | 107.29 | |
| | 75 | 0 | 4.0x10 ⁻⁶ | 8.0x10 ⁻⁶ | 12.0x10 ⁻⁶ | 3.14x10 ⁻⁴ | 3.88x10 ⁻⁴ | 4.35x10 ⁻⁴ | 1.76x10 ⁶ | 1.92x10 ⁶ | 1.96x10 ⁶ | CHF | CHF | CHF | |
| | | | 6.0x10 ⁻⁶ | 12.0x10 ⁻⁶ | 18.0x10 ⁻⁶ | 4.79x10 ⁻⁴ | 5.90x10 ⁻⁴ | 6.62x10 ⁻⁴ | 2.14x10 ⁶ | 2.33x10 ⁶ | 2.38x10 ⁶ | 122.12 | 120.44 | 119.54 | |
| | | | 8.0x10 ⁻⁶ | 16.0x10 ⁻⁶ | 24.0x10 ⁻⁶ | 6.45x10 ⁻⁴ | 7.95x10 ⁻⁴ | 8.92x10 ⁻⁴ | 2.46x10 ⁶ | 2.67x10 ⁶ | 2.73x10 ⁶ | 119.74 | 118.14 | 117.29 | |
| 211.4 | 85 | 60 | 25 | 4.0x10 ⁻⁶ | 8.0x10 ⁻⁶ | 12.0x10 ⁻⁶ | 1.89x10 ⁻⁴ | 2.33x10 ⁻⁴ | 2.60x10 ⁻⁴ | 2.12x10 ⁶ | 2.31x10 ⁶ | 2.36x10 ⁶ | 115.39 | 113.41 | 112.40 |
| | | | | 6.0x10 ⁻⁶ | 12.0x10 ⁻⁶ | 18.0x10 ⁻⁶ | 2.88x10 ⁻⁴ | 3.54x10 ⁻⁴ | 3.96x10 ⁻⁴ | 2.58x10 ⁶ | 2.81x10 ⁶ | 2.87x10 ⁶ | 111.47 | 109.66 | 108.70 |
| | | | | 8.0x10 ⁻⁶ | 16.0x10 ⁻⁶ | 24.0x10 ⁻⁶ | 3.88x10 ⁻⁴ | 4.77x10 ⁻⁴ | 5.34x10 ⁻⁴ | 2.96x10 ⁶ | 3.22x10 ⁶ | 3.30x10 ⁶ | 108.87 | 107.15 | 106.23 |
| | 65 | 20 | 4.0x10 ⁻⁶ | 8.0x10 ⁻⁶ | 12.0x10 ⁻⁶ | 1.89x10 ⁻⁴ | 2.33x10 ⁻⁴ | 2.60x10 ⁻⁴ | 2.10x10 ⁶ | 2.29x10 ⁶ | 2.34x10 ⁶ | 120.39 | 118.41 | 117.40 | |
| | | | 6.0x10 ⁻⁶ | 12.0x10 ⁻⁶ | 18.0x10 ⁻⁶ | 2.88x10 ⁻⁴ | 3.54x10 ⁻⁴ | 3.96x10 ⁻⁴ | 2.56x10 ⁶ | 2.79x10 ⁶ | 2.85x10 ⁶ | 116.47 | 114.66 | 113.70 | |
| | | | 8.0x10 ⁻⁶ | 16.0x10 ⁻⁶ | 24.0x10 ⁻⁶ | 3.88x10 ⁻⁴ | 4.77x10 ⁻⁴ | 5.34x10 ⁻⁴ | 2.94x10 ⁶ | 3.20x10 ⁶ | 3.27x10 ⁶ | 113.87 | 112.15 | 111.23 | |
| | 75 | 10 | 4.0x10 ⁻⁶ | 8.0x10 ⁻⁶ | 12.0x10 ⁻⁶ | 1.89x10 ⁻⁴ | 2.33x10 ⁻⁴ | 2.60x10 ⁻⁴ | 2.07x10 ⁶ | 2.26x10 ⁶ | 2.31x10 ⁶ | 130.39 | 128.41 | 127.40 | |
| | | | 6.0x10 ⁻⁶ | 12.0x10 ⁻⁶ | 18.0x10 ⁻⁶ | 2.88x10 ⁻⁴ | 3.54x10 ⁻⁴ | 3.96x10 ⁻⁴ | 2.52x10 ⁶ | 2.74x10 ⁶ | 2.80x10 ⁶ | 126.47 | 124.66 | 123.70 | |
| | | | 8.0x10 ⁻⁶ | 16.0x10 ⁻⁶ | 24.0x10 ⁻⁶ | 3.88x10 ⁻⁴ | 4.77x10 ⁻⁴ | 5.34x10 ⁻⁴ | 2.90x10 ⁶ | 3.15x10 ⁶ | 3.22x10 ⁶ | 123.87 | 122.15 | 121.23 | |
| | 85 | 0 | 4.0x10 ⁻⁶ | 8.0x10 ⁻⁶ | 12.0x10 ⁻⁶ | 1.89x10 ⁻⁴ | 2.33x10 ⁻⁴ | 2.60x10 ⁻⁴ | 2.04x10 ⁶ | 2.22x10 ⁶ | 2.27x10 ⁶ | 140.39 | 138.41 | 137.40 | |
| | | | 6.0x10 ⁻⁶ | 12.0x10 ⁻⁶ | 18.0x10 ⁻⁶ | 2.88x10 ⁻⁴ | 3.54x10 ⁻⁴ | 3.96x10 ⁻⁴ | 2.48x10 ⁶ | 2.70x10 ⁶ | 2.76x10 ⁶ | 136.47 | 134.66 | 133.70 | |
| | | | 8.0x10 ⁻⁶ | 16.0x10 ⁻⁶ | 24.0x10 ⁻⁶ | 3.88x10 ⁻⁴ | 4.77x10 ⁻⁴ | 5.34x10 ⁻⁴ | 2.85x10 ⁶ | 3.10x10 ⁶ | 3.17x10 ⁶ | 133.87 | 132.15 | 131.23 | |

Table 4. Continued.

| P _{sat} (kPa) | T _{sat} (°C) | T _f (°C) | ΔT _{sub} (°C) | Q (m ³ /s) | | | B | | | CHF (W/m ²) | | | T _s (°C) at 200 W/cm ² | | |
|---------------------------|--------------------------|------------------------|---------------------------|--------------------------|-----------------------|-----------------------|-----------------------|-----------------------|-----------------------|----------------------------|----------------------|----------------------|--|----------|----------|
| | | | | Nozzle 1 | Nozzle 2 | Nozzle 3 | Nozzle 1 | Nozzle 2 | Nozzle 3 | Nozzle 1 | Nozzle 2 | Nozzle 3 | Nozzle 1 | Nozzle 2 | Nozzle 3 |
| 275.9 | 95 | 60 | 35 | 4.0x10 ⁻⁶ | 8.0x10 ⁻⁶ | 12.0x10 ⁻⁶ | 1.18x10 ⁻⁴ | 1.45x10 ⁻⁴ | 1.63x10 ⁻⁴ | 2.45x10 ⁶ | 2.67x10 ⁶ | 2.72x10 ⁶ | 120.11 | 118.00 | 116.83 |
| | | | | 6.0x10 ⁻⁶ | 12.0x10 ⁻⁶ | 18.0x10 ⁻⁶ | 1.79x10 ⁻⁴ | 2.20x10 ⁻⁴ | 2.48x10 ⁻⁴ | 2.98x10 ⁶ | 3.25x10 ⁶ | 3.32x10 ⁶ | 115.91 | 113.94 | 112.83 |
| | | | | 8.0x10 ⁻⁶ | 16.0x10 ⁻⁶ | 24.0x10 ⁻⁶ | 2.42x10 ⁻⁴ | 2.97x10 ⁻⁴ | 3.34x10 ⁻⁴ | 3.42x10 ⁶ | 3.73x10 ⁶ | 3.81x10 ⁶ | 113.06 | 111.20 | 110.16 |
| | | 65 | 30 | 4.0x10 ⁻⁶ | 8.0x10 ⁻⁶ | 12.0x10 ⁻⁶ | 1.18x10 ⁻⁴ | 1.45x10 ⁻⁴ | 1.63x10 ⁻⁴ | 2.44x10 ⁶ | 2.66x10 ⁶ | 2.71x10 ⁶ | 125.11 | 123.00 | 121.83 |
| | | | | 6.0x10 ⁻⁶ | 12.0x10 ⁻⁶ | 18.0x10 ⁻⁶ | 1.79x10 ⁻⁴ | 2.20x10 ⁻⁴ | 2.48x10 ⁻⁴ | 2.97x10 ⁶ | 3.23x10 ⁶ | 3.30x10 ⁶ | 120.91 | 118.94 | 117.83 |
| | | | | 8.0x10 ⁻⁶ | 16.0x10 ⁻⁶ | 24.0x10 ⁻⁶ | 2.42x10 ⁻⁴ | 2.97x10 ⁻⁴ | 3.34x10 ⁻⁴ | 3.40x10 ⁶ | 3.70x10 ⁶ | 3.79x10 ⁶ | 118.06 | 116.20 | 115.16 |
| | | 75 | 20 | 4.0x10 ⁻⁶ | 8.0x10 ⁻⁶ | 12.0x10 ⁻⁶ | 1.18x10 ⁻⁴ | 1.45x10 ⁻⁴ | 1.63x10 ⁻⁴ | 2.41x10 ⁶ | 2.62x10 ⁶ | 2.68x10 ⁶ | 135.11 | 133.00 | 131.83 |
| | | | | 6.0x10 ⁻⁶ | 12.0x10 ⁻⁶ | 18.0x10 ⁻⁶ | 1.79x10 ⁻⁴ | 2.20x10 ⁻⁴ | 2.48x10 ⁻⁴ | 2.93x10 ⁶ | 3.19x10 ⁶ | 3.26x10 ⁶ | 130.91 | 128.94 | 127.83 |
| | | | | 8.0x10 ⁻⁶ | 16.0x10 ⁻⁶ | 24.0x10 ⁻⁶ | 2.42x10 ⁻⁴ | 2.97x10 ⁻⁴ | 3.34x10 ⁻⁴ | 3.36x10 ⁶ | 3.66x10 ⁶ | 3.74x10 ⁶ | 128.06 | 126.20 | 125.16 |
| | | 85 | 10 | 4.0x10 ⁻⁶ | 8.0x10 ⁻⁶ | 12.0x10 ⁻⁶ | 1.18x10 ⁻⁴ | 1.45x10 ⁻⁴ | 1.63x10 ⁻⁴ | 2.38x10 ⁶ | 2.59x10 ⁶ | 2.64x10 ⁶ | 145.11 | 143.00 | 141.83 |
| | | | | 6.0x10 ⁻⁶ | 12.0x10 ⁻⁶ | 18.0x10 ⁻⁶ | 1.79x10 ⁻⁴ | 2.20x10 ⁻⁴ | 2.48x10 ⁻⁴ | 2.90x10 ⁶ | 3.15x10 ⁶ | 3.22x10 ⁶ | 140.91 | 138.94 | 137.83 |
| | | | | 8.0x10 ⁻⁶ | 16.0x10 ⁻⁶ | 24.0x10 ⁻⁶ | 2.42x10 ⁻⁴ | 2.97x10 ⁻⁴ | 3.34x10 ⁻⁴ | 3.32x10 ⁶ | 3.62x10 ⁶ | 3.70x10 ⁶ | 138.06 | 136.20 | 135.16 |
| | | 95 | 0 | 4.0x10 ⁻⁶ | 8.0x10 ⁻⁶ | 12.0x10 ⁻⁶ | 1.18x10 ⁻⁴ | 1.45x10 ⁻⁴ | 1.63x10 ⁻⁴ | 2.35x10 ⁶ | 2.56x10 ⁶ | 2.61x10 ⁶ | 155.11 | 153.00 | 151.83 |
| | | | | 6.0x10 ⁻⁶ | 12.0x10 ⁻⁶ | 18.0x10 ⁻⁶ | 1.79x10 ⁻⁴ | 2.20x10 ⁻⁴ | 2.48x10 ⁻⁴ | 2.86x10 ⁶ | 3.11x10 ⁶ | 3.18x10 ⁶ | 150.91 | 148.94 | 147.83 |
| | | | | 8.0x10 ⁻⁶ | 16.0x10 ⁻⁶ | 24.0x10 ⁻⁶ | 2.42x10 ⁻⁴ | 2.97x10 ⁻⁴ | 3.34x10 ⁻⁴ | 3.28x10 ⁶ | 3.57x10 ⁶ | 3.65x10 ⁶ | 148.06 | 146.20 | 145.16 |

REPORT DOCUMENTATION PAGE

Form Approved
OMB No. 0704-0188

The public reporting burden for this collection of information is estimated to average 1 hour per response, including the time for reviewing instructions, searching existing data sources, gathering and maintaining the data needed, and completing and reviewing the collection of information. Send comments regarding this burden estimate or any other aspect of this collection of information, including suggestions for reducing the burden, to Department of Defense, Executive Services and Communications Directorate (0704-0188). Respondents should be aware that notwithstanding any other provision of law, no person shall be subject to any penalty for failing to comply with a collection of information if it does not display a currently valid OMB control number.

PLEASE DO NOT RETURN YOUR FORM TO THE ABOVE ORGANIZATION.

| | | | | | | | | |
|--|------------------------------------|-------------------------------------|---|----------------------------|--|-------------------------------------|--|--|
| 1. REPORT DATE (DD-MM-YYYY) July 2008 | | | 2. REPORT TYPE Conference Paper | | | 3. DATES COVERED (From - To) | | |
| 4. TITLE AND SUBTITLE Two-Phase Spray Cooling of Hybrid Vehicle Electronics: Preprint | | | | | 5a. CONTRACT NUMBER DE-AC36-99-GO10337 | | | |
| | | | | | 5b. GRANT NUMBER | | | |
| | | | | | 5c. PROGRAM ELEMENT NUMBER | | | |
| 6. AUTHOR(S) I. Mudawar: Mudawar Thermal Systems; D. Bharathan, K. Kelly, and S. Narumanchi: NREL | | | | | 5d. PROJECT NUMBER NREL/CP-540-42389 | | | |
| | | | | | 5e. TASK NUMBER FC087000 | | | |
| | | | | | 5f. WORK UNIT NUMBER | | | |
| 7. PERFORMING ORGANIZATION NAME(S) AND ADDRESS(ES) National Renewable Energy Laboratory 1617 Cole Blvd. Golden, CO 80401-3393 | | | | | 8. PERFORMING ORGANIZATION REPORT NUMBER NREL/CP-540-42389 | | | |
| 9. SPONSORING/MONITORING AGENCY NAME(S) AND ADDRESS(ES) | | | | | 10. SPONSOR/MONITOR'S ACRONYM(S) NREL | | | |
| | | | | | 11. SPONSORING/MONITORING AGENCY REPORT NUMBER | | | |
| 12. DISTRIBUTION AVAILABILITY STATEMENT National Technical Information Service U.S. Department of Commerce 5285 Port Royal Road Springfield, VA 22161 | | | | | | | | |
| 13. SUPPLEMENTARY NOTES | | | | | | | | |
| 14. ABSTRACT (Maximum 200 Words) As part of the U.S. Department of Energy's Advanced Power Electronics activities, the National Renewable Energy Laboratory is leading a national effort to develop next-generation cooling technologies for hybrid vehicle electronics. Spray cooling is a potential solution that can dissipate 150 to 200 watts per square centimeter while maintaining the chip temperature below 125 degrees C. This study explores the viability and implementation of this cooling scheme. Commercial coolants are assessed for their suitability in terms of thermal, environmental, and safety concerns and material compatibility, and HFE-7100 is identified as the optimum coolant in all performance categories. Spray models are used to determine the HFE-7100 spray conditions that meet stringent heat dissipation requirements. The findings are verified experimentally, demonstrating that spray cooling is a viable thermal management solution for hybrid vehicle electronics. | | | | | | | | |
| 15. SUBJECT TERMS hybrid electric vehicles; vehicle power electronics; spray cooling; vehicle thermal management | | | | | | | | |
| 16. SECURITY CLASSIFICATION OF: | | | 17. LIMITATION OF ABSTRACT UL | 18. NUMBER OF PAGES | 19a. NAME OF RESPONSIBLE PERSON | | | |
| a. REPORT Unclassified | b. ABSTRACT Unclassified | c. THIS PAGE Unclassified | | | 19b. TELEPHONE NUMBER (Include area code) | | | |